ADVANCED FUNCTIONAL MATERIALS
www.afm-journal.de

Materials Views
www.MaterialsViews.com

On Intensifying Carrier Impurity Scattering to Enhance Thermoelectric Performance in Cr-Doped $Ce_yCo_4Sb_{12}$

Shanyu Wang, Jiong Yang, Lihua Wu, Ping Wei, Wenqing Zhang, and Jihui Yang**

The beneficial effect of impurity scattering on thermoelectric properties has long been disregarded even though possible improvements in power factor have been suggested by Ioffe more than a half century ago. Here it is theoretically and experimentally demonstrated that proper intensification of ionized impurity scattering to charge carriers can benefit the thermoelectric figure of merit (*ZT*) by increasing the Seebeck coefficient and decreasing the electronic thermal conductivity. The optimal strength of ionized impurity scattering for maximum *ZT* depends on the Fermi level and the density of states effective mass. Cr-doping in $Ce_yCo_4Sb_{12}$ progressively increases the strength of ionized impurity scattering, and significantly improves the Seebeck coefficient, resulting in high power factors of 45 μW cm^{-1} K^{-2} with relatively low electrical conductivity. This effect, combined with the increased Ce-filling fraction and thus decreased lattice thermal conductivity by charge compensation of Cr-dopant, gives rise to a maximum *ZT* of 1.3 at 800 K and a large average *ZT* of 1.1 between 500 and 850 K, ≈30% and ≈20% enhancements as compared with those of Cr-free sample, respectively. Furthermore, this study also reveals that carrier scattering parameter can be another fundamental degree of freedom to optimize electrical properties and improve thermal-to-electricity conversion efficiencies of thermoelectric materials.

1. Introduction

Thermoelectric technology is currently limited to niche applications, and this is primarily due to the low performance of the state-of-the-art materials.[1,2] The thermoelectric performance of a material is quantified by a dimensionless figure of merit, $ZT = \alpha^2\sigma T/\kappa$, where α, σ, κ, and T are the Seebeck coefficient, electrical conductivity, thermal conductivity, and the absolute temperature in Kevin, respectively. Strengthening phonon scattering to lower lattice thermal conductivity κ_L through nanostructures,[3,4] lattice anharmonicity,[5] alloying,[6,7] atomic rattling,[8] point defect engineering,[9] etc., has led to fruitful achievements in thermoelectrics. However, in many instances κ_L has already been lowered to the amorphous limit, suggesting that further enhancement in *ZT* should come from the improvement of power factor ($PF = \alpha^2\sigma$) or the decrease in electronic thermal conductivity.[10] Strategies such as carrier concentration engineering[2,11] and band structure modification[12] have been identified to be effective for *PF* and *ZT* enhancements.

Besides being pertinent to the electronic band structure and the Fermi level, electrical transport properties are also closely related to the carrier scattering processes, including phonon scattering, impurity scattering, energy barrier scattering, etc.[13–15] Above room temperature, lattice vibrations generally dominate the carrier scattering for most of the thermoelectric materials, e.g., Bi_2Te_3[16] or PbTe.[17] Since almost all of the thermoelectric materials are heavily doped semiconductors, impurity scattering, especially ionized impurity scattering, could play an important role in carrier transport at $T > 300$ K, as evident in Ni-doped[18,19] or Te-doped[20] $CoSb_3$, or transition metal-substituted clathrates.[21] The carrier scattering probability by ionized impurity is inversely proportional to $\varepsilon^{3/2}$ (ε: carrier energy) or v^3 (v: drift velocity),[22,23] therefore the low energy carriers would experience more scattering and be filtered out by the charged impurities. This energy filtering effect could enhance the Seebeck coefficient, analogous to the effect of energy barriers.[3,15] Theoretically this offers the possibility to optimize *PF* through balancing the mobility decrease and the Seebeck coefficient enhancement, and the optimal scattering parameter should depend on the Fermi level and other material-specific parameters.[14,18,24] This effect is analogue to the prediction by Ioffe[25] about a half century ago, however, rather precise control of the impurity scattering strength is required to realize power factor and *ZT* improvements in heavily doped semiconductors.[26] Indeed, Ioffe's initial experimental work about PbTe gave no enhancement in power factor or *ZT*,[25] and subsequently numerical calculations done by Ure[24] predicted no more than 10% enhancement in *ZT* by introducing ionized impurities. These may have contributed to the dormancy of studying the influence of ionized impurity scattering on thermoelectrics, and to the best of our knowledge only limited experimental results have been reported.[18,27]

The strength of ionized impurity scattering depends not only on the effective concentration of impurities but also on

Dr. S. Wang, Dr. J. Yang, Dr. L. Wu,
Dr. P. Wei, Prof. J. Yang
Material Science and Engineering Department
University of Washington
Seattle, WA 98195, USA
E-mail: jihuiy@uw.edu
Prof. W. Zhang
Materials Genome Institute
Shanghai University
Shanghai 200444, P. R. China
E-mail: wqzhang@mail.sic.ac.cn

DOI: 10.1002/adfm.201502782

the carrier concentration and some other material-specific parameters, such as the dielectric constant K, density of states effective mass m_d*. According to Brooks' and Herring's derivations,[23,28] the carrier relaxation time of ionized impurity scattering under the Born approximation and a Coulombic potential screening effect is expressed as

$$\tau_I = \frac{K^2\left(2m_d^*\right)^{\frac{1}{2}}\varepsilon^{\frac{3}{2}}}{\pi e^4 N_I}\left[\ln(1+b)-\frac{b}{1+b}\right]^{-1}, b=\frac{2Km_d^* k_B T\varepsilon}{\pi\hbar^2 e^2 n'} \quad (1)$$

where e, N_I, k_B, and $\hbar$ are the elementary charge, effective impurity density, the Boltzmann constant, and the reduced Planck constant, respectively. n' is related to the carrier concentration n and charge compensation (when both acceptors and donors are present), and equal to n if a single type of impurity is present (such as the donors in an n-type semiconductor). It is obvious that the carrier screening effect (proportional to K) and charge compensation (b) both influence τ_I significantly. For materials with large K values, such as PbTe ($K \sim 1000$), the ionized impurity scattering seldom plays an important role in carrier transport.[15,17] Furthermore, it can be noted that the last term in the bracket of Equation (1), which can be simplified as $[\ln(1+b)-1]^{-1}$ when $b >> 1$ (the Born approximation[29]), is a function of the degree of charge compensation which depends on the concentrations of donors, acceptors, and charge carriers.

Although ionized impurity scattering has been intensively studied,[14,18,22,23,29–31] its effect on the electrical properties in the context of thermoelectricity has seldom been emphasized or quantitatively investigated.[24,25] To the best of our knowledge, the original prediction by Ioffe[25] has seldom been explicitly demonstrated experimentally. In the present study, by assuming the carrier transport being dominated by a mixed acoustic phonon and ionized impurity scatterings, we numerically illustrate that an increase in the strength of ionized impurity scattering could moderately improve the power factor by balancing the enhancement in Seebeck coefficient and the reduction of mobility, and thus appreciably enhance ZT for a given lattice thermal conductivity. This concept is further experimentally validated in Cr-doped $Ce_yCo_4Sb_{12}$ samples prepared by a traditional melting–annealing–sintering technique. Here Cr-doping at the Co sites has two effects: (i) adjusting the strength of ionized impurity scattering through increasing impurity concentration, and (ii) increasing Ce filling fraction limit (FFL) by charge compensation. The low FFL of Ce (≈0.1) in $CoSb_3$ is insufficient to optimize the electrical properties (the optimal doping concentration is ≈0.5e per Co_4Sb_{12}, corresponding to y of ≈0.17 for Ce) or reduce κ_L.[32,33] The charge compensation provided by Cr at the Co sites or other acceptors (Fe, Mn at the Co sites[33,34] or Sn, Ge at the Sb sites[35,36] is an effective approach to adjust carrier concentration and reduce κ_L by increasing FFL, primarily due to the strong filler–defect interaction which stabilizes the fillers.[33,36] More importantly, enhanced Seebeck coefficients owing to the intensified impurity scattering render high power factors over a wide temperature range. This high average power factor coupled with the decreased κ_L gives rise to a maximum ZT of ≈1.3 and a large average ZT of 0.9 between 300 and 850 K, which are ≈30% and ≈20% improvement over those of Cr-free sample, respectively.

2. Results and Discussion

2.1. Cr Charge Compensation and Its Effects on Electrical Properties at 300 K

Powder X-ray diffraction (XRD) shown in Figure S1 (Supporting Information) indicates that the main phase is the cubic skutterudite (space group *Im*-3), and all samples contain minor Sb phase. The backscattered images shown in Figure S2 (Supporting Information), however, feature minute microsize Ce-rich precipitates (CeSb or $CeSb_2$, <1 vol%) due to the low FFL of Ce in $CoSb_3$ (≈0.1). The amount of Ce-rich precipitates decreases with increasing Cr content owing to the charge compensation effect of Cr at the Co sites, which increases the Ce filling fraction as indicated by the energy-dispersive X-ray spectroscopy (EDX) derived Ce content in **Table 1** (the EDX-derived Ce content increases gradually from 0.09 to 0.14). Concurrently, electron concentration shown in Table 1 increases gradually with increasing Cr-content, mainly because of the increase in the Ce filling fraction that overcompensates the substitutional acceptor Cr_{Co} in $CoSb_3$. The "overcompensation" phenomena can also be found in Fe-doped and Mn-doped Ce-filled skutterudites,[33,34] as well as other n-type filled skutterudites with other p-type acceptors

Table 1. The EDX-derived Ce content, density (ρ), lattice parameters (a_0), carrier concentrations (n_H), Hall mobilities (μ_H), Seebeck coefficient (α), reduced Fermi energy (η), effective mass (m_d^*/m_0), and lattice thermal conductivity (κ_L) at 300 K for $Ce_yCo_{4-x}Cr_xSb_{12}$ (x = 0–0.1; y = 0.2, 0.25) compounds.

Samples	Ce content	ρ [g cm^{-3}]	a_0 [Å]	n_H [10^{20} cm^{-3}]	μ_H [cm^2 V^{-1} s^{-1}]	α [μV K^{-1}]	η	m_d^*/m_0	κ_L [W m^{-1} K^{-1}]
$Ce_{0.2}Co_4$	0.09	7.56	9.0428	1.9	34	−160	0.98	2.84	3.2
$Ce_{0.2}Cr_{0.025}$	0.12	7.53	9.0425	1.9	36	−160	1.02	2.86	3.1
$Ce_{0.2}Cr_{0.05}$	0.13	7.57	9.0474	3.0	28	−145	1.49	3.17	2.3
$Ce_{0.2}Cr_{0.1}$	0.13	7.31	9.0462	3.0	20	−170	1.48	3.16	2.3
$Ce_{0.25}Co_4$	0.10	7.63	9.0460	2.1	42	−151	1.12	2.93	2.4
$Ce_{0.25}Cr_{0.025}$	0.12	7.47	9.0438	2.3	39	−152	1.21	2.99	2.3
$Ce_{0.25}Cr_{0.05}$	0.14	7.36	9.0463	2.7	32	−149	1.39	3.10	2.2
$Ce_{0.25}Cr_{0.1}$	0.14	7.50	9.0474	2.7	25	−168	1.38	3.10	2.1

(defects).[35,36] The origin of these results is the filler–defect interaction which further stabilizes the fillers and therefore enhances the FFL, as pointed out in ref.[37]. **Figure 1**a shows the interaction energy between Ce and transition metal defects, versus the defect charge states. The interaction energy is obtained by the energy differences between the configurations with the dopant at the nearest site to Ce and at a nonnearest site. The computational details can be found in ref.[37]. Cr_{Co}, Mn_{Co}, and Fe_{Co} all have beneficial interaction energies with the fillers in Co_4Sb_{12}, which well accounts for the general overcompensation phenomenon. The interaction energy roughly increases linearly with the defect charge state as shown in Figure 1a, implying that the interaction is Coulombic in nature. In fact, due to the attraction between Ce and Cr_{Co}, their nearest distance is ≈3.65 Å, slightly shorter than that of Ce–Co (3.88 Å). The interaction energy of the Ce–Cr_{Co} (0.19 eV) is close to that of the Ce–Ga_{Sb} (0.21 eV),[37] even though the Co site is much further away than the nearest Sb site. This is presumably due to the high charge state of the Cr_{Co}, which significantly influences the transport properties of the host as discussed below. It is worthwhile noting that the starting stoichiometry particularly that of Sb or high annealing temperature may significantly influence the FFL of Ce in $CoSb_3$, as recently suggested by Tang et al.,[38] but these are not applicable in this study as all samples are stoichiometric in Co and Sb and the same annealing temperature was used for each sample.

Besides increasing the Ce-filling fraction and electron concentration, Cr-doping also significantly influences carrier transport properties, such as the scattering mechanism, etc. Electron mobility decreases rapidly with increasing carrier concentration, especially for the $x = 0.1$ samples. Figure 1b shows mobility versus carrier concentration for all $Ce_yCo_{4-x}Cr_xSb_{12}$ samples, which are obviously lower than the general trend of filled $CoSb_3$.[32] The very low mobilities for the Cr-doped samples indicate either intensified phonon scattering or the introduction of additional scattering mechanisms, e.g., impurity scattering. The α–n plot of Cr-doped samples does not follow the general trend of filled $CoSb_3$,[39] especially for the $x = 0.1$ samples, as shown in Figure 1c. The physical model based on single parabolic band and acoustic phonon scattering (SPB-AS) approximation also fails to predict the Seebeck coefficient variations of Cr-doped samples, as indicated as the dotted line in Figure 1c with $m_d^* = 3.0m_0$ (Pisarenko relation). Assuming a

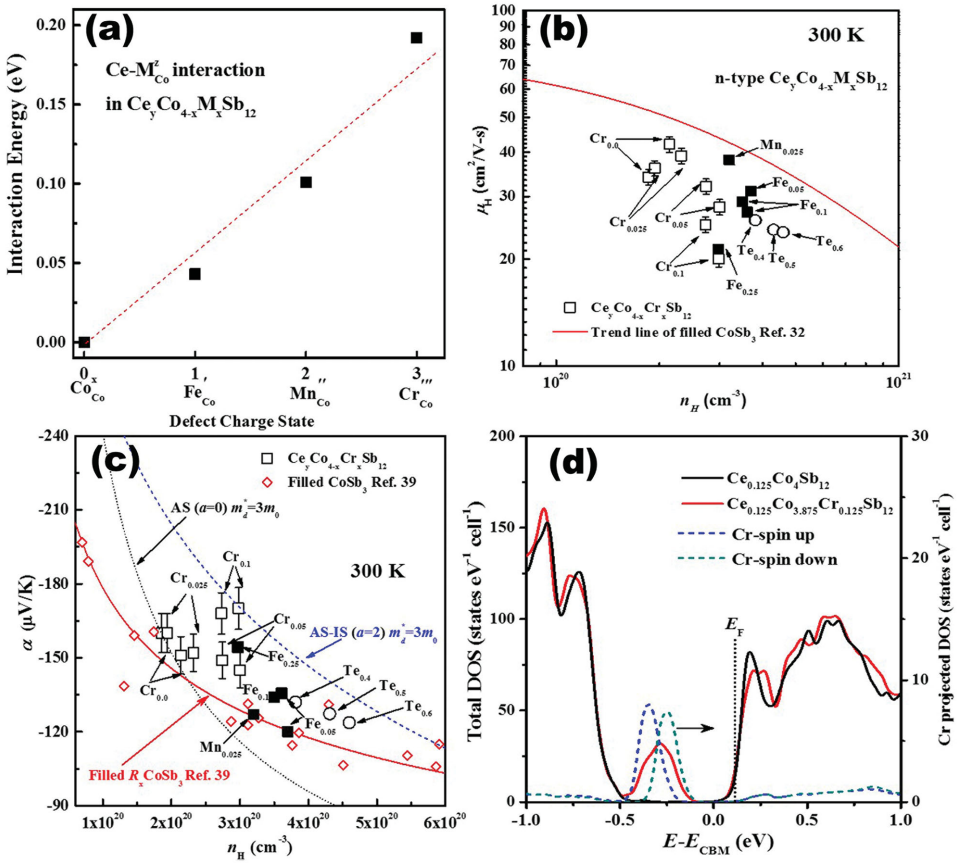

Figure 1. a) The filler–defect interaction energy in M-doped and Ce-filled $Ce_yCo_{4-x}M_xSb_{12}$ (M = Fe, Mn, and Cr) as a function of defect charge state. b) Electron mobility as a function of carrier concentration at 300 K for $Ce_yCo_{4-x}Cr_xSb_{12}$, and the solid line is the trend of filled skutterudites taken from ref. [32]. c) Seebeck coefficient as a function of carrier concentration at 300 K for $Ce_yCo_{4-x}Cr_xSb_{12}$. The experimental data of Fe-,[33,34] Mn-,[33] and Te-doped[40] $CoSb_3$ are also shown in (b) and (c). The diamond points and solid line are for filled $CoSb_3$ taken from ref. [39], and the dotted and dashed lines are calculated by assuming single parabolic band (SPB) and acoustic phonon scattering (AS ($a = 0$), $m_d^* = 3m_0$) as well as SPB and mixed ionized impurity and acoustic phonon scattering (AS-IS ($a = 2$), $m_d^* = 3m_0$), respectively. The error bars in (b) and (c) are 5%. d) Total density of states (DOS) for $Ce_{0.125}Co_4Sb_{12}$ and $Ce_{0.125}Co_{3.875}Cr_{0.125}Sb_{12}$, with spin polarization considered for the latter. DOS projections on Cr for both spins are also shown. The vertical dotted line represents the Fermi level position when the electron concentration equals to 3×10^{20} cm^{-3}.

mixed scattering of acoustic phonon and ionized impurity scattering (a = 2, see the Experimental Section) and the same SPB with $m_d^* = 3.0m_0$, the calculated α–n relation is also plotted as the dashed line in Figure 1c. It should be noted that the SPB assumption would introduce some errors in determining the Fermi energy due to the nonparabolic nature of conduction band, however, in the present study the m_d^* values inputted into the calculations were captured by the Kane model which are well consistent with the trend of filled $CoSb_3$, as indicated as the red solid line in Figure 1c. The α–n points of Cr-doped samples move progressively from the dotted (a = 0) line to the dashed line (a = 2), indicating a gradual increase in the proportion of ionized impurity scattering with increasing Cr content. Similar mobility reduction and Seebeck coefficient enhancement can be found for Fe-doped or Te-doped samples,[33,34,40] as shown in Figure 1b,c. In addition, the first principles density of states (DOS) for $Ce_{0.125}Co_{3.875}Cr_{0.125}Sb_{12}$ and $Ce_{0.125}Co_4Sb_{12}$ were calculated, as shown in Figure 1d. Cr atom introduces localized d states at the top of the valence band, with 0.1 eV energy splitting under spin polarization. These localized states are 0.2 eV higher than those in Fe-based p-type skutterudites[41] due to the less-d-electron nature of Cr. In the conduction band, Cr d states are much more dispersive due to the strong d–p hybridization with the Sb atoms, and have negligible contributions to the total DOS. As shown in Figure 1d, the total DOS for samples with or without Cr are almost identical in the energy window of 0–0.15 eV above the conduction band bottom, which is the typical range for n-type filled skutterudites.[42] According to the above analyses, it can be concluded that the Seebeck coefficient enhancement should be mainly originated from the variation of electron scattering mechanism, such as the introduction of impurity scattering which increases the average electron entropy (kinetic energy)[7] or spin-electron scattering associated with the unpaired electrons of Cr ions. Significant Seebeck coefficient improvement has indeed been observed previously by varying the carrier scattering mechanism in PbTe[13,15] and Sb_2Te_3.[43]

2.2. Numerical Modeling of the Effect of Ionized Impurity Scattering on the Electrical Properties

To explore the variation of scattering parameter and its effects on the electrical transport properties, high temperature Hall coefficient R_H (300–700 K) was measured, as shown in **Figure 2**a. R_H decreases rapidly with increasing temperature which has been reported for lots of filled skutterudites.[44] The rapid decrease in R_H, starting at very low temperatures

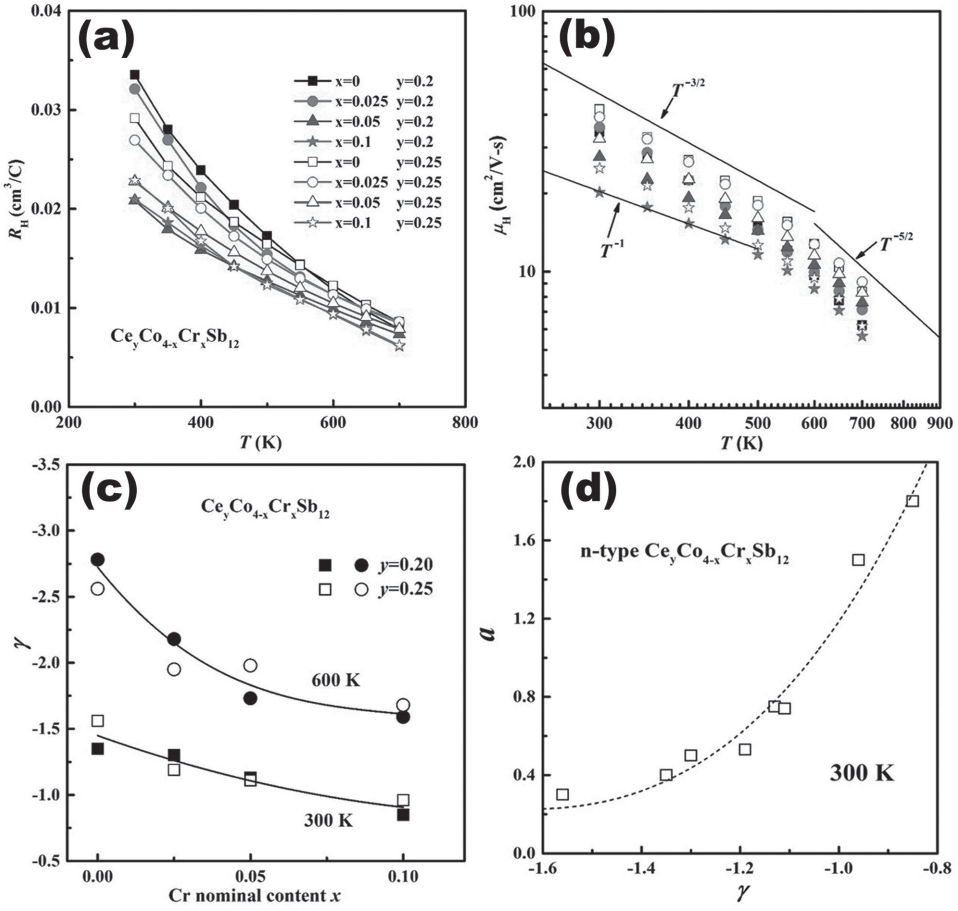

Figure 2. Temperature dependences of a) Hall coefficient R_H and b) carrier mobility μ_H of $Ce_yCo_{4-x}Cr_xSb_{12}$; c) temperature exponents γ of mobility around 300 and 600 K; d) calculated ionized impurity scattering index a as a function of γ. Lines in Figure 2c,d are guides for the eye.

(≈10 K), is distinct from normal degenerate semiconductors, and the origin of this phenomenon is unclear.[14] The bipolar conduction, only appeared at elevated temperatures (>700 K) as evident for the temperature dependent Seebeck coefficient and lattice thermal conductivity shown below, should be irrelevant for the anomalous temperature dependence of Hall coefficient in present study (300–700 K). Figure 2b shows the temperature dependence of mobility, and the Cr-free samples show temperature exponents γ of ≈–1.5 around 300 K, indicative of acoustic phonon scattering of the carriers. With increasing Cr content, however, γ around 300 K varies gradually to ≈–0.9 for the x = 0.1 samples, as shown in Figure 2c. This indicates a gradual increase in strength of the ionized impurity scattering, which can be further attributed to the substitutional Cr ions at the Co sites, similar to the effect of Ni-doping.[18,19] Yang et al. had studied the valence state of Cr in $CoSb_3$ and concluded that Cr takes the Cr^{3+} state, and thus the total number of valence electrons does not change with Cr-doping.[45] In this study, however, increase in Ce filling fraction for Cr-doped samples indicates a charge compensation and the acceptor role of Cr in Ce_yCoSb_3, similar to the effects of Fe-doping or Mn-doping at the Co site[33,34] or Sn-doping or Ge-doping at the Sb site.[35,36] This further suggests a divalent (Cr^{2+}) or monovalent (Cr^{+}) charge state of Cr which acts as charge scattering centers. The discrepancy is presumably due to the different Fermi levels, and the high chemical potential of our Ce-filled samples may drive Cr into lower valence states (Cr^{2+} or Cr^{+}). More experiments, however, are needed to clarify the detailed valence state of Cr, such as magnetic susceptibility. Meanwhile, since τ_I is proportional to $T^{3/2}$, the strength of ionized impurity scattering decreases gradually with rising temperature, as evidenced by the rapid increase of $|\gamma|$ with increasing temperature, and phonon scattering begins to dominate carrier transport at T > 500 K. The sharp decrease of mobility at elevated temperatures (T > 600 K, $\mu_H \sim T^{-2.5}$) is presumably due to the polar optical phonon scattering, intervalley scattering, or intensified electron–hole coupling.[46]

The ionized impurity scattering indexes (a) are numerically solved from the Seebeck coefficient and carrier concentration, and are plotted as a function of γ in Figure 2d. The methodology is presented in the Experimental Section below. It is obvious that the calculated a value increases monotonically with decreasing $|\gamma|$, indicating that the enhancement in Seebeck coefficient is mainly originated from variation of scattering mechanism. Assuming the Fermi level η = 1 ($n = 1.9 \times 10^{20}$ cm^{-3}), electrical transport properties as functions of a at 300 K are shown in **Figure 3**a. The electrical conductivity decreases while the Seebeck coefficient increases correspondingly with increasing a. In particular, the power factor first increases and then decreases with the intensifying ionized

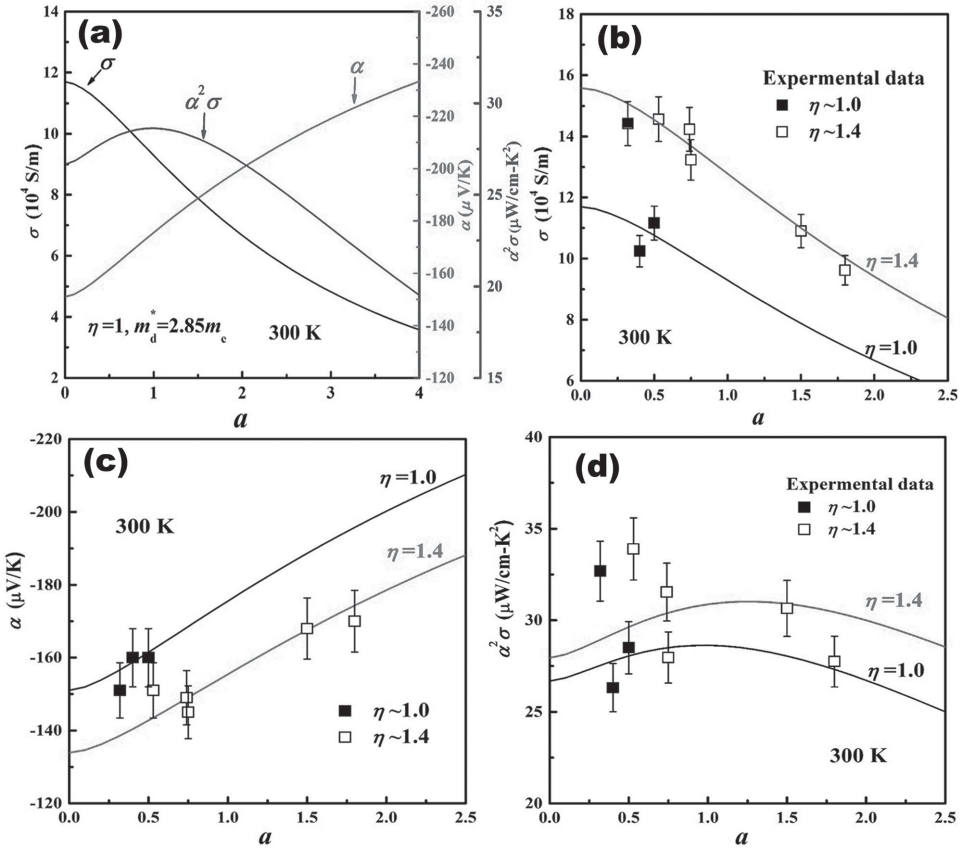

Figure 3. a) The modeled electrical transport properties of n-type skutterudites at 300 K as functions of the ionized impurity scattering index a. b–d) Comparisons of the experimental data of $Ce_yCo_{4-x}Cr_xSb_{12}$ at 300 K with those calculated trend lines for electrical conductivity, Seebeck coefficient, and power factor. The error bars in (b–d) are all 5%.

impurity scattering, peaking at $a = a_0$ (PF enhances by ≈7.3%). $a_0 \approx 1$ while Fermi energy $\eta = 1$, and increases with increasing η, for example $a_0 = 2.4$ for $\eta = 2$ ($n = 4.6 \times 10^{20}$ cm^{-3}). This result agrees well with the predictions of Ioffe[25] and Ure.[24] The increase in the Seebeck coefficient, due to the filtering of low-energy electrons by ionized impurity scattering, compensates or even overcompensates the reduction of mobility, giving rise to the power factor enhancement. This effect is in principle analogues to the filtering effect created by energy barriers.[3] Particularly, thermal conductivity can also be lowered due to the reduced electronic contribution and the intensified phonon point defect scattering, and thus a large enhancement in ZT can be expected. The comparisons between the experimental data and the numerical calculations (solid lines) are shown in Figure 3b–d. These calculations without any adjustable parameter show good agreement with the experimental results, especially for the Seebeck coefficient and the electrical conductivity. The discrepancies are mainly attributed to the variation of the Fermi level, as indicated in Table 1. This further verifies the rationality of the present simple model. The fits between calculated and experimental power factors are less satisfactory, mainly due to the variation of η and large uncertainty of PF (≈10%). Intensification of ionized impurity scattering does not noticeably deteriorate the power factor, especially for the $x = 0.1$ samples with very low electrical conductivities.

2.3. High Temperature Thermoelectric Transport Properties

The high temperature electrical transport properties of $Ce_{0.25}Co_{4-x}Cr_xSb_{12}$ samples are shown in **Figure 4**, and the experimental results of $Ce_{0.2}Co_{3.9}Fe_{0.1}Sb_{12}$ ($a = 0.55$, $\eta = 1.66$) and $Ce_{0.2}Co_{3.875}Mn_{0.025}Sb_{12}$ ($a = 0.0$, $\eta = 1.56$) from ref.[33] are also presented for comparison. To exclude the influence of Fermi energy variation and explicitly demonstrate the effects of ionized impurity scattering on thermoelectric properties, the transport properties of a hypothetical sample with same Fermi energy as the $x = 0.1$ sample ($\eta = 1.38$) and predominant acoustic phonon scattering (same a value as $Ce_{0.25}Co_4Sb_{12}$, $a = 0.3$) were calculated and are shown as the red dashed lines (σ and α take identical temperature dependence as those of $Ce_{0.25}Co_4Sb_{12}$). The transport properties of $Ce_{0.2}Co_{4-x}Cr_xSb_{12}$ are shown in Figure S3 (Supporting Information). The electrical conductivity shown in Figure 4a first remains unchanged due to the counterbalance between the increase of electron concentration and the decrease of mobility, and then decreases for the $x = 0.1$ sample owing to the apparent mobility reduction by ionized impurity scattering. The strong ionized impurity scattering can also be inferred by the different temperature dependences of σ, especially for the $x = 0.1$ sample. The hypothetical $x = 0.1$ sample with the predominant acoustic phonon scattering ($a = 0.3$, $\eta = 1.38$) indeed shows high mobility and conductivity. Figure 4b displays the temperature dependences of the Seebeck coefficient for $Ce_{0.2}Co_{4-x}Cr_xSb_{12}$. Cr-doped samples with increased Fermi energies, especially the $x = 0.1$ sample with large a value, show largely enhanced Seebeck coefficients, mainly due to the intensified ionized impurity scattering. The Seebeck coefficient enhancement prevails in the entire temperature range, as compared with the much lower overall Seebeck coefficient of the hypothetical

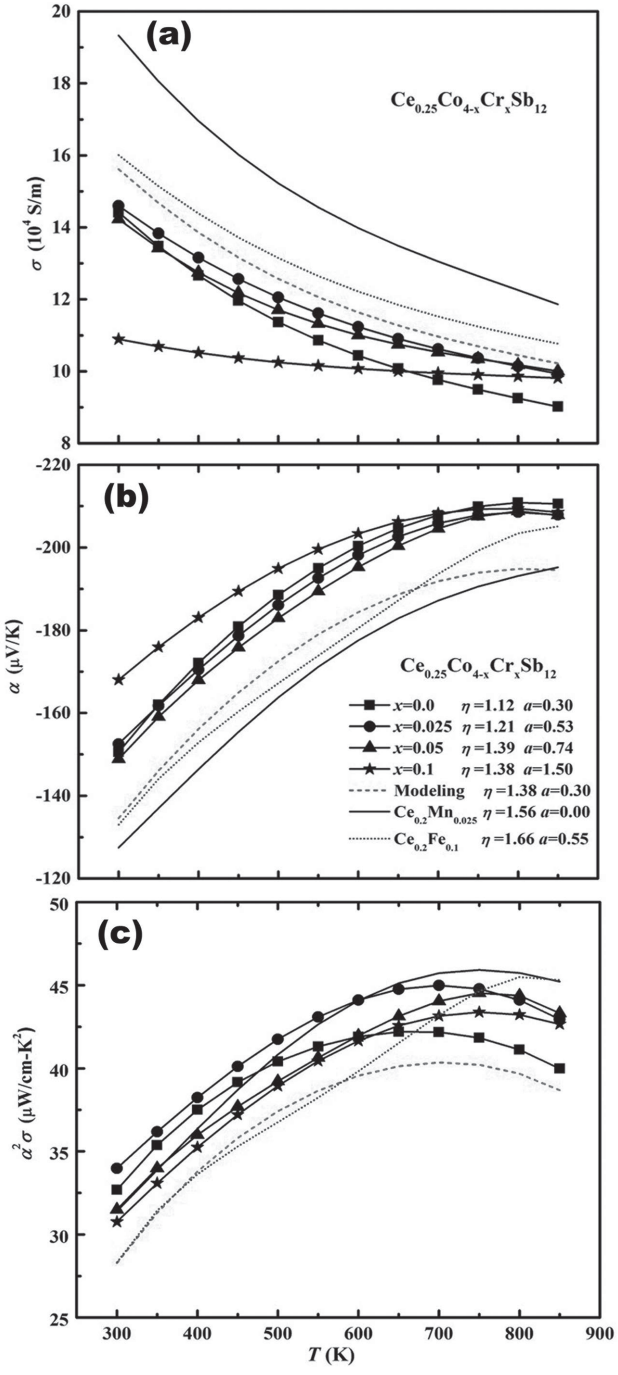

Figure 4. Temperature dependences of thermoelectric transport properties of $Ce_{0.25}Co_{4-x}Cr_xSb_{12}$ samples, a) electrical conductivity, b) Seebeck coefficient, c) power factor. Electrical properties of the hypothetical $x = 0.1$ sample ($a = 0.3$, $\eta = 1.38$) with a predominant acoustic phonon scattering, Mn- and Fe-doped $Ce_{0.2}Co_4Sb_{12}$[33] are shown as the dashed, solid, and dotted lines, respectively.

$x = 0.1$ sample ($a = 0.3$, $\eta = 1.38$). The high temperature Seebeck coefficients ($T > 700$ K) of Cr-doped samples are comparable to those of $Ce_{0.25}Co_4Sb_{12}$, even though the later possesses much lower η, as shown in Table 1. $Ce_{0.2}Co_{3.875}Mn_{0.025}Sb_{12}$ with a dominant acoustic phonon scattering ($a = 0$, $\eta = 1.56$) shows high σ

due to its high mobility, whereas $Ce_{0.2}Co_{3.9}Fe_{0.1}Sb_{12}$ (a = 0.55, η = 1.66) displays lower σ even with higher Fermi energy because of the intensified ionized impurity scattering.[33] This intensification of ionized impurity scattering also gives larger Seebeck coefficients in the whole temperature range for $Ce_{0.2}Co_{3.9}Fe_{0.1}Sb_{12}$ (a = 0.55, η = 1.66), analogue to the effect of Cr-doping in the present study. The enhanced Seebeck coefficients ensure high power factors over a wide temperature range, as shown in Figure 4c. Cr-doped samples show moderate enhancement in the power factor, and the maximum value reaches 45 μW cm^{-1} K^{-2} which is comparable to those best results of Ce single filled $CoSb_3$.[33,38] It is further noted that the x = 0.1 sample (a = 1.5, η = 1.38) shows ≈5%–10% *PF* enhancement in the whole temperature range over the hypothetical x = 0.1 sample (a = 0.3, η = 1.38), consistent with the predications of Ioffe[25] and Ure[24] and in the present study.

Thermal transport properties of $Ce_{0.25}Co_{4-x}Cr_xSb_{12}$ are shown in **Figure 5**, and those of Mn-doped and Fe-doped $Ce_{0.2}Co_4Sb_{12}$ and the hypothetical x = 0.1 sample (a = 0.3, η = 1.38) are also shown as the solid, dotted, and dashed lines for comparison, respectively. κ of the hypothetical x = 0.1 sample (a = 0.3, η = 1.38) was calculated by summing the experimental κ_L of the x = 0.1 sample (a = 1.5, η = 1.38) and the calculated electronic contribution κ_e. κ_e was estimated based on the Wiedemann–Franz law, $\kappa_e = L\sigma T$, where L is the Lorenz constant and taken as 2.0 × 10^{-8} V^2 K^{-2}. κ decreases gradually with the increasing Cr content x, attributed to the decrease of both the electronic and the lattice contributions, as shown in Figure 5b,c. κ_L first decreases with rising temperature due to the intensified phonon–phonon Umklapp processes, and then increases slightly at elevated temperatures because of the bipolar contribution.[47] More importantly, κ_L decreases gradually with the increasing Cr content due to the increased Ce filling fraction. κ_L of Cr-doped samples is comparable to those of Fe-doped or Mn-doped $Ce_{0.2}Co_4Sb_{12}$,[33] as shown in Figure 5c. κ_L at 300 K as a function of filling fraction of Ce,[33,48] Yb,[49] alkaline, and alkaline earth[50] are shown Figure 5d. Our experimental results fit well with the trend line of Ce-filled $CoSb_3$.[33,48] This indicates that the increase in Ce filling fraction is the dominant source of κ_L reduction, and phonon defect

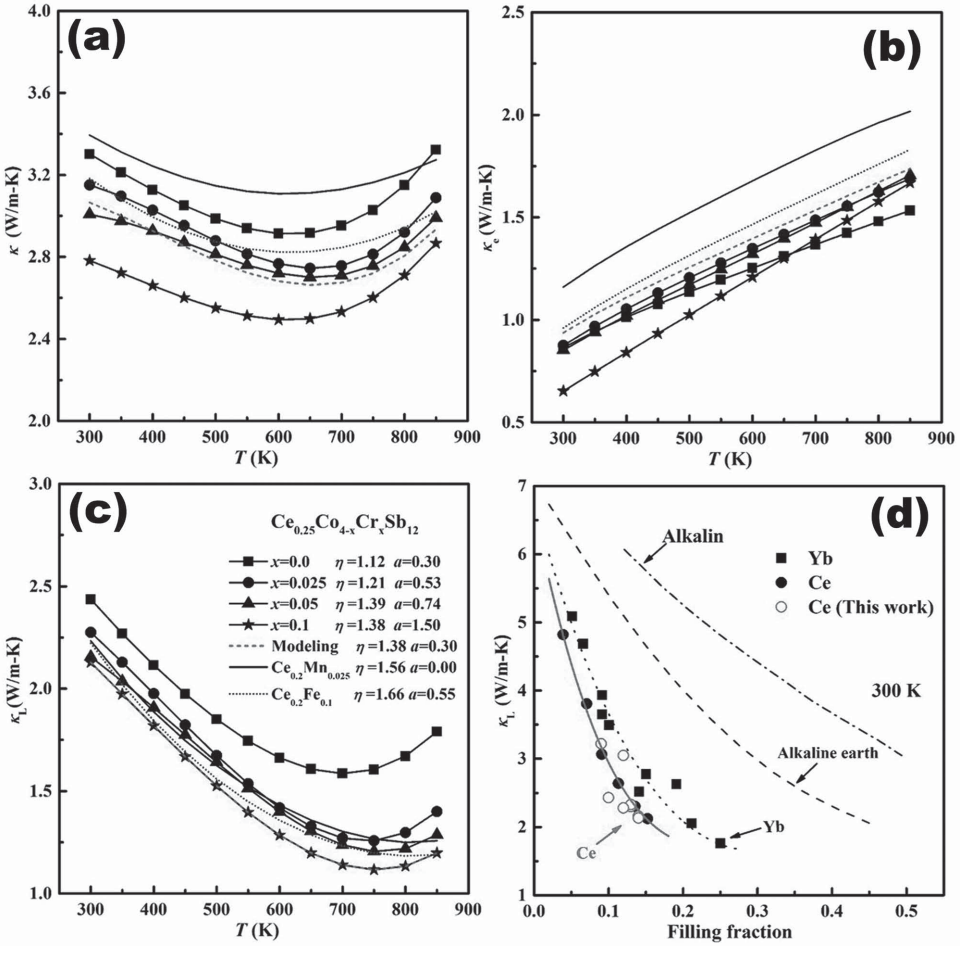

Figure 5. Temperature dependences of a) thermal conductivity, b) electronic thermal conductivity, and c) lattice thermal conductivity for $Ce_{0.25}Co_{4-x}Cr_xSb_{12}$. Thermal properties of the hypothetical x = 0.1 sample (a = 0.3, η = 1.38) with a predominant acoustic phonon scattering, Mn- and Fe-doped $Ce_{0.2}Co_4Sb_{12}$[33] are shown as the dashed, solid, and dotted lines, respectively. d) Lattice thermal conductivity at 300 K as a function of filling fraction for $Ce_yCo_{4-x}Cr_xSb_{12}$, and the filled circles of Ce-filled Co_4Sb_{12} are previous reported results[33,48] (the solid line is a guide to the eye). The trend lines of alkali-filled, alkaline-earth-filled, and Yb-filled Co_4Sb_{12}[49] are also shown for comparison.

scattering due to Cr-substitution at the Co sites is negligible in light of their comparable atomic masses and sizes. Compared with other fillers, Ce is one of the most effective filler for κ_L reduction due to its low rattling frequency (54 cm^{-1}).[51] The low filling fraction of Ce (~0.1) in undoped $CoSb_3$, however, limits κ_L reduction and power factor optimization.[51] The charge compensation provided by Fe or Mn,[33] or by Cr in this study is an effective way to increase Ce filling fraction, which in turn optimizes carrier concentration and lowers κ_L.

Thermoelectric figure of merit ZT at 300 K as a function of ionized impurity scattering index a is shown in **Figure 6**a, together with the results of the hypothetical $x = 0.1$ sample ($a = 0.3$, $\eta = 1.38$), as well as the Fe-doped and Mn-doped $Ce_{0.2}Co_4Sb_{12}$ in ref.[33]. Considering the inevitable variations of the Fermi level and lattice thermal conductivity, the agreement between the theoretical model and experimental data is acceptable. As argued, proper intensification of the ionized impurity scattering indeed increases ZT, e.g., ZT maximizes at $a \approx 1.6$ with $\eta = 1.4$ ($n = 2.8 \times 10^{20}$ cm^{-3}). The temperature dependences of ZTs for $Ce_{0.25}Co_{4-x}Cr_xSb_{12}$ are shown in Figure 6b. Cr-doping gradually increases ZT and the maximum value reaches ≈1.3 for the $x = 0.1$ sample ($a = 1.5$, $\eta = 1.38$), ≈30% improvement as compared with that of $Ce_{0.25}Co_4Sb_{12}$. This maximum ZT is also comparable to those of the Fe-doped $Ce_{0.2}Co_4Sb_{12}$[33] and the best values of single-filled skutterudites,[51,52] and also ≈15% higher than that of the hypothetical $x = 0.1$ sample with the dominant acoustic phonon scattering for electrons ($a = 0.3$, $\eta = 1.38$). In particular, the average ZT, crucial for the conversion efficiency of thermoelectric devices, is also appreciably improved, as shown in Figure 6c. The average ZT of 0.9 between 300 and 850 K ($\overline{ZT}_{300-850K}$) for the $x = 0.1$ sample is ≈17% and ≈14% higher than those of the undoped and the hypothetical $x = 0.1$ ($a = 0.3$, $\eta = 1.38$) samples, respectively. Even with comparable maximum ZT as the Fe-doped sample, the $x = 0.1$ sample ($a = 1.5$, $\eta = 1.38$) shows more than 10% higher $\overline{ZT}_{300-850K}$ and $\overline{ZT}_{500-850K}$. The high ZT and average ZT are mainly originated from the intensified ionized impurity scattering which ensures high α and PF in a wide temperature range, as well as reduced κ from both the lattice and the electronic contributions. Although the ZT enhancement is modest considering the measurement errors (≈15%), the good reproducibility and agreement with theoretical predications of thermoelectric transport properties explicitly demonstrate the beneficial effect of ionized impurity scattering, which can be applied for other materials to achieve more significant ZT enhancement. We further trust that even higher ZT can be achieved by optimizing the carrier concentration and/or impurity scattering index a, as well as by further decreasing κ_L via multiple filling in $CoSb_3$ skutterudites.

2.4. Some Further Discussion about the Strategy of Ionized Impurity Scattering

It is believed that the strategy utilizing ionized impurity scattering to enhance thermoelectric properties can be widely applied to many other thermoelectric compounds, such as Bi_2Te_3, Mg_2Si, etc. The key to the strategy is how to effectively introduce ionized impurity scattering and how to precisely control its proportion to realize PF and ZT enhancements. According to Equation (1), large effective impurity concentration N_I and small m_d^* are necessary to produce strong ionized impurity scattering for a material with a small enough K value (<100). Here N_I is not only determined by the concentration of impurity centers N_i (dopants) but also their charge states v, and roughly proportional to v^2N_i.[22,23] Thus a highly charged impurity with high screened Coulomb potential will more effectively scatter low energy electrons, and give rise to higher electron entropy and higher Seebeck coefficient. This also accounts for the stronger ionized impurity scattering introduced by Cr_{Co} defects, in comparison with Fe_{Co} or Mn_{Co}, as shown in Figure 1a–c. In addition, another factor influencing the ionized impurity scattering strength is the characteristics of electronic band structure. In general, the ionized impurities located at the carrier transporting sublattices would more pronouncedly scatter the charge carriers. Therefore for n-type $CoSb_3$, doping at the Co sites such as Ni, Fe, Cr, etc., more effectively introduces ionized impurity scattering, due to the fact that the conduction band bottom is mainly composed of transition metal d orbitals and some contributions from Sb p orbitals through the p–d hybridization.[41] Te-doping at the Sb sites, even with high dopant concentrations, has very limited effect on carrier scattering mechanism, as shown in Figure 1b,c.[20,40] In addition, the m_d^* for a given material has a limited room to adjust, and also seldom becomes a dominant parameter for ionized impurity scattering (also shown as square root in relaxation or mobility formulas, Equation (1)).

The optimal proportion of ionized impurity scattering strongly depends on the Fermi energy (carrier concentration) and other parameters such as m_d^*, and the concurrent dependence of Fermi energy and ionized impurity scattering strength on N_I make precise control rather challenging. The difficulty is also responsible for many unsuccessful attempts.[7,27] Advanced theoretical calculations and sophisticated experiments are needed to control the ionized impurity scattering strength and the Fermi energy. Special attention should be paid to the preparation of polycrystalline samples, which may contain high density intrinsic defects, such as vacancies, interstitials, or antisite defects. These intrinsic defects may significantly alter the scattering processes of charge carriers.

3. Conclusions

In this study, we have demonstrated that proper intensification of the ionized impurity scattering can be an effective approach to improve the electrical transport properties and thermoelectric figure of merit ZT in n-type Cr-doped $Ce_yCo_4Sb_{12}$. Here Cr-doping not only intensifies the ionized impurity scattering and efficiently increases the Seebeck coefficient, ensuring high power factors, but also noticeably reduces the lattice thermal conductivity by increasing the Ce filling fraction. A highest ZT of ≈1.3 can be achieved for $Ce_{0.25}Co_{3.9}Cr_{0.1}Sb_{12}$, ≈30% improvement over the Cr-free sample, and also comparable to the best values of single-filled $CoSb_3$. In addition, the large average ZTs of 0.9 between 300 and 850 K as well as 1.1 between 500 and 850 K can be achieved with an optimal a value of 1.5, ≈15% higher than those of the sample assuming a dominant acoustic phonon

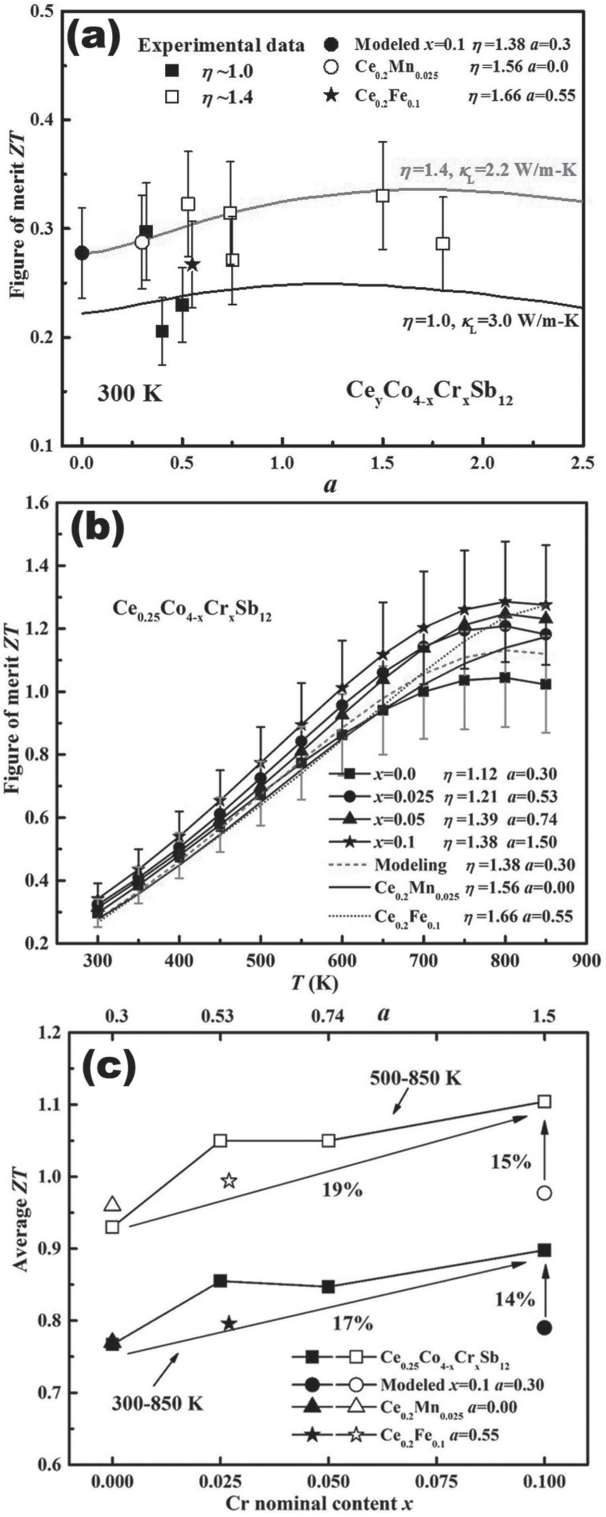

Figure 6. a) Comparison of experimental *ZT* with calculations (solid lines) at 300 K; b) temperature dependences of *ZT* for $Ce_{0.25}Co_{4-x}Cr_xSb_{12}$. The error bars in (a) and (b) are 15%. c) Average *ZT* between 300 and 850 K as well as between 500 and 850 K. *ZT* values of the hypothetical $x = 0.1$ sample with a predominant acoustic phonon scattering ($a = 0.3$, $\eta = 1.38$), experimental data for $Ce_{0.2}Co_{3.9}Fe_{0.1}Sb_{12}$ ($a = 0.55$, $\eta = 1.66$) and $Ce_{0.2}Co_{3.975}Mn_{0.025}Sb_{12}$ ($a = 0$, $\eta = 1.56$) taken from ref. [33] are also shown.

scattering ($a = 0.3$). We believe that this strategy can be applied for improving *ZT* of double- or triple-filled skutterudites or other thermoelectric compounds, by feasibly combining with other strategies such as band structure engineering, energy barrier filtering, nanostructuring, etc.

4. Experimental Section

Sample Synthesis and Characterization: All samples were prepared according to the stoichiometry $Ce_\gamma Co_{4-x}Cr_xSb_{12}$ ($x = 0$–0.1; $\gamma = 0.2$, 0.25) by a conventional melting–quenching–annealing–sintering method. High purity Co shots (99.995%, Alfa Aesar), Cr chunks (99.99%, Sigma Aldrich), Sb shots (99.999%, Alfa Aesar), and Ce chunks (99.95%, Alfa Aesar) were weighed stoichiometrically, loaded into carbon-coated quartz tubes in an argon-filled glove-box (Mbraun, lab star, Germany) and vacuum sealed (10^{-3} Torr). The tubes with raw materials were placed into a box furnace, heated to 1100 °C in 5 h, soaked at this temperature for 24 h, and then rapidly quenched in ice water. The obtained ingots were ultrasonically cleaned and vacuum sealed in quartz tubes, then annealed in a box furnace at 750 °C for 168 h. After annealing, the ingots were crushed, hand grounded into fine powders and sintered into bulk materials using spark plasma sintering at ≈650 °C and 50 MPa for 5 min. 1.5–2 mm thick circular sheets with diameter 12.7 mm, $3 \times 3 \times 12$ mm^3, and $0.3 \times 2.5 \times 8$ mm^3 rectangular bars were cut for thermoelectric properties and Hall effect measurements.

The phase purities of bulk samples were determined by powder XRD (Bruker D8 Focus X-ray diffraction) using the Cu K_α radiation (λ = 1.5406 Å), and lattice parameters were calculated using the full profile Rietveld refinement method in the FullProf_Suite software. Backscattered electron images were collected in a Hitachi TM3000 electron microscope equipped with a Bruker EDX. The chemical compositions were determined by an FEI Sirion field emission scanning electron microscope equipped with EDX (FESEM/EDX). The electrical conductivity (σ) and Seebeck coefficient (α) were simultaneously measured by a commercial equipment (ZEM-3, Ulvac Riko, Inc.) under a low-pressure helium atmosphere. Thermal conductivity (κ) was calculated from the measured thermal diffusivity (λ), specific heat (C_p), and density (d) using the relationship $\kappa = \lambda C_p d$. Thermal diffusivity λ was tested by the laser flash method using a Netzsch LFA-457 system, and specific heat (C_p) was measured by a Netzsch DSC 404F1 using sapphire as the reference. The measurement temperature ranges from 300 to 850 K. Uncertainties in electrical conductivity, Seebeck coefficient, thermal conductivity, and *ZT* are estimated to be ±5%, ±3%, ±10%, and ±15%, respectively. The high temperature Hall coefficient measurements (300–700 K) were performed on a home-made Hall system equipped with a 2 T electromagnet, with a four-probe configuration. Carrier concentration (n_H) and Hall mobility (μ_H) were determined from the measured Hall coefficient (R_H) and electrical conductivity by the relation $n_H = r/e|R_H|$ (assuming the Hall factor r as 1.0) and $\mu_H = \sigma|R_H|$.

Numerical Calculations: Based on the assumption that carrier transport is dominated by a mixed scattering of acoustic phonon ($\tau_L = \tau_{0,L}\varepsilon^{-1/2}$) and ionized impurity ($\tau_i = \tau_{0,i}\varepsilon^{3/2}$), the combined relaxation time can be expressed as

$$\tau = \frac{\tau_{0,L}\varepsilon^{3/2}}{\varepsilon^2 + a^2} \tag{2}$$

where $a = \sqrt{\frac{\tau_{0,L}}{\tau_{0,i}}}$ is defined as the ionized impurity scattering index

$$\tau_{0,L} = \frac{\pi N_v \hbar^4 C_{ll}}{\sqrt{2}\Xi^2 \left(m_b^* k_B T\right)^{3/2}} \tag{3}$$

where N_v, C_{ll}, Ξ, and m_b^* are the band degeneracy, average longitudinal elastic constant, the band deformation potential, and the density of state effective mass of a single band, respectively. Neutral impurity scattering and electron–electron couplings are not considered in the present study.

The neutral impurity scattering should be negligible at high temperatures compared with lattice or ionized impurity scattering.[23,53] Electron–electron couplings, tending to randomize drift velocity of electrons, could be rather effective when ionized impurity scattering dominates in carrier transport, as suggested by Herring or Debye.[23] The effect of electron–electron couplings had been discussed in detail elsewhere by Debye and Conwell.[23,31] In this study we neglect the effect of electron–electron couplings, and detailed discussion of their effect is beyond the scope of present study. In addition, we did not use the Brooks–Herring formula or other variants to quantitatively describe the strength of ionized impurity scattering, due to the break-down of the Brooks–Herring formula at high impurity level ($N_I > 10^{17}$ cm^{-3}) and high temperatures ($T > 300$ K).[31]

Under the relaxation time approximation for mixed lattice and ionized impurity scatterings and SPB assumption, the transport equations as functions of the reduced Fermi level η and ionized impurity scattering index a are expressed as

$$\sigma(\eta,a) = \frac{8\pi(m_d^*)^{1/2}e^2}{3h^3}(2k_BT)^{3/2}\tau_{0,L}\Phi_3(\eta,a) \quad (4)$$

$$\alpha(\eta,a) = -\frac{k_B}{e}\left[\frac{\Phi_4(\eta,a)}{\Phi_3(\eta,a)} - \eta\right] \quad (5)$$

$$\mu = \frac{2e}{3m_d^*}\tau_{0,L}\frac{\Phi_3(\eta,a)}{F_{1/2}(\eta)} \quad (6)$$

$$n = 4\pi\left(\frac{2m_d^*k_BT}{h^2}\right)^{3/2}F_{1/2}(\eta) \quad (7)$$

$$L(\eta,a) = \left(\frac{k_B}{e}\right)^2\frac{\Phi_4(\eta,a)^2 - \Phi_3(\eta,a)\Phi_5(\eta,a)}{\Phi_3(\eta,a)^2} \quad (8)$$

$$\text{and } \Phi_m(\eta,a) = \int_0^\infty \frac{\varepsilon^m\exp(\varepsilon-\eta)}{(\varepsilon^2+a^2)\left[1+\exp(\varepsilon-\eta)\right]^2}d\varepsilon \quad (9)$$

where $F_{1/2}(\eta)$ is the Fermi integral of the order of 1/2. For given η and κ_L, the electrical transport properties as functions of ionized impurity scattering index a ($a \geq 0$) can be numerically calculated. Some physical parameters used for calculations were taken from literatures, such as $C_{ll} = 1.5\times10^{11}$ GPa,[54] Ξ = 6.5 eV,[55] and N_v = 3 for the conduction band.[56]

First-Principles Calculations: All first-principles calculations were performed with the Vienna *ab initio* simulation package.[57] Generalized gradient approximation functional[58] and projected augmented wave methods[59] were used. We adopted a $2 \times 2 \times 2$ supercell of the Co_4Sb_{12} unit in all the calculations, which is large enough for the defect study in skutterudites.[37] Spin-polarization is considered in the electronic structure calculations.

Supporting Information

Supporting Information is available from the Wiley Online Library or from the author.

Acknowledgements

The authors thank Dr. Feiyue Ma and Prof. Jiangyu Li in Mechanical Engineering Department at University of Washington for the kind help in high temperature Hall measurements. Jiong Yang thanks Dr. Lili Xi from Shanghai Institute of Ceramics, Chinese Academy of Sciences and Dr. Yubo Zhang from Temple University for helpful discussions. This work was supported by US Department of Energy under corporate agreement DE-FC26-04NT42278 and by GM, and by National Science Foundation under award number 1235535.

Received: July 7, 2015
Revised: August 16, 2015
Published online: October 8, 2015

[1] J. Yang, H. L. Yip, A. K. Y. Jen, *Adv. Energy Mater.* **2013**, *3*, 549.
[2] G. J. Snyder, E. S. Toberer, *Nat. Mater.* **2008**, *7*, 105.
[3] M. S. Dresselhaus, G. Chen, M. Y. Tang, R. Yang, H. Lee, D. Wang, Z. Ren, J. P. Fleurial, P. Gogna, *Adv. Mater.* **2007**, *19*, 1043.
[4] a) Y. Lan, A. J. Minnich, G. Chen, Z. Ren, *Adv. Funct. Mater.* **2010**, *20*, 357; b) C. J. Vineis, A. Shakouri, A. Majumdar, M. G. Kanatzidis, *Adv. Mater.* **2010**, *22*, 3970.
[5] a) S. Wang, J. Yang, L. Wu, P. Wei, J. Yang, W. Zhang, Y. Grin, *Chem. Mater.* **2015**, *27*, 1071; b) D. Morelli, V. Jovovic, J. Heremans, *Phys. Rev. Lett.* **2008**, *101*, 035901.
[6] H. J. Goldsmid, *J. Appl. Phys.* **1961**, *32*, 2198.
[7] A. Joffe, *Can. J. Phys.* **1956**, *34*, 1342.
[8] a) G. Nolas, D. Morelli, T. M. Tritt, *Annu. Rev. Mater. Sci.* **1999**, *29*, 89; b) J. Cohn, G. Nolas, V. Fessatidis, T. Metcalf, G. Slack, *Phys. Rev. Lett.* **1999**, *82*, 779; c) B. Sales, D. Mandrus, R. K. Williams, *Science* **1996**, *272*, 1325.
[9] a) L. Hu, T. Zhu, X. Liu, X. Zhao, *Adv. Funct. Mater.* **2014**, 24, 5211; b) G. Jiang, J. He, T. Zhu, C. Fu, X. Liu, L. Hu, X. Zhao, *Adv. Funct. Mater.* **2014**, *24*, 3776.
[10] J. Zhang, R. Liu, N. Cheng, Y. Zhang, J. Yang, C. Uher, X. Shi, L. Chen, W. Zhang, *Adv. Mater.* **2014**, *26*, 3848.
[11] Y. Pei, A. D. LaLonde, N. A. Heinz, X. Shi, S. Iwanaga, H. Wang, L. Chen, G. J. Snyder, *Adv. Mater.* **2011**, *23*, 5674.
[12] a) Y. Pei, X. Shi, A. LaLonde, H. Wang, L. Chen, G. J. Snyder, *Nature* **2011**, *473*, 66; b) W. Liu, X. Tan, K. Yin, H. Liu, X. Tang, J. Shi, Q. Zhang, C. Uher, *Phys. Rev. Lett.* **2012**, *108*, 166601.
[13] J. P. Heremans, C. M. Thrush, D. T. Morelli, *Phys. Rev. B* **2004**, *70*, 115334.
[14] V. I. Fistul, *Heavily Doped Semiconductors*, Vol. *1*, Plenum Press, New York, NY, USA **1969**.
[15] J. Martin, L. Wang, L. Chen, G. Nolas, *Phys. Rev. B* **2009**, *79*, 115311.
[16] a) S. Wang, G. Tan, W. Xie, G. Zheng, H. Li, J. Yang, X. Tang, *J. Mater. Chem.* **2012**, *22*, 20943; b) W. Xie, J. He, H. J. Kang, X. Tang, S. Zhu, M. Laver, S. Wang, J. R. Copley, C. M. Brown, Q. Zhang, *Nano Lett.* **2010**, *10*, 3283.
[17] R. S. Allgaier, W. W. Scanlon, *Phys. Rev.* **1958**, *111*, 1029.
[18] J. S. Dyck, W. Chen, C. Uher, L. Chen, X. Tang, T. Hirai, *J. Appl. Phys.* **2002**, *91*, 3698.
[19] J. S. Dyck, W. Chen, J. Yang, G. P. Meisner, C. Uher, *Phys. Rev. B* **2002**, *65*, 115204.
[20] X. Li, L. Chen, J. Fan, W. Zhang, T. Kawahara, T. Hirai, *J. Appl. Phys.* **2005**, *98*, 083702.
[21] X. Shi, J. Yang, S. Bai, J. Yang, H. Wang, M. Chi, J. R. Salvador, W. Zhang, L. Chen, W. Wong-Ng, *Adv. Funct. Mater.* **2010**, *20*, 755.
[22] D. Chattopadhyay, H. Queisser, *Rev. Mod. Phys.* **1981**, *53*, 745.
[23] P. Debye, E. Conwell, *Phys. Rev.* **1954**, *93*, 693.
[24] R. W. Ure Jr., *J. Appl. Phys.* **1959**, *30*, 1922.
[25] A. F. Ioffe, *Semiconductor Thermoelements and Thermoelectric Cooling*, Infosearch, London, UK **1957**.
[26] H. Goldsmid, *Materials* **2014**, *7*, 2577.
[27] Y. Pei, L. Chen, S. Bai, X. Zhao, X. Li, *Scrip. Mater.* **2007**, *56*, 621.
[28] H. Brooks, *Advances in Electronics and Electron Physics*, Academic Press, Inc., New York, NY, USA **1955**.
[29] E. Conwell, V. Weisskopf, *Phys. Rev.* **1950**, *77*, 388.
[30] F. Gamiz, J. López-Villanueva, *J. Appl. Phys.* **1995**, *78*, 1787.
[31] D. Long, J. Myers, *Phys. Rev.* **1959**, *115*, 1107.
[32] X. Shi, J. Yang, J. R. Salvador, M. Chi, J. Y. Cho, H. Wang, S. Bai, J. Yang, W. Zhang, L. Chen, *J. Am. Chem. Soc.* **2011**, *133*, 7837.
[33] P. Qiu, X. Shi, Y. Qiu, X. Huang, S. Wan, W. Zhang, L. Chen, J. Yang, *Appl. Phys. Lett.* **2013**, *103*, 062103.
[34] C. Uher, C.-P. Li, S. Ballikaya, *J. Electron. Mater.* **2010**, *39*, 2122.

[35] G. Lamberton Jr., R. Tedstrom, T. Tritt, G. Nolas, *J. Appl. Phys.* **2005**, *97*, 113715.
[36] J. Yang, D. Morelli, G. Meisner, W. Chen, J. Dyck, C. Uher, *Phys. Rev. B* **2003**, *67*, 165207.
[37] L. Xi, Y. Qiu, X. Shi, W. Zhang, D. Singh, J. Yang, *Chem. Comm.* **2015**, *51*, 10823.
[38] Y. Tang, R. Hanus, S.-W. Chen, G. J. Snyder, *Nat. Commun.* **2015**, *6*, 7584.
[39] S. Bai, Y. Pei, L. Chen, W. Zhang, X. Zhao, J. Yang, *Acta Mater.* **2009**, *57*, 3135.
[40] B. Duan, P. Zhai, L. Liu, Q. Zhang, X. Ruan, *J. Solid State Chem.* **2012**, *193*, 8.
[41] J. Yang, P. Qiu, R. Liu, L. Xi, S. Zheng, W. Zhang, L. Chen, D. J. Singh, J. Yang, *Phys. Rev. B* **2011**, *84*, 235205.
[42] J. Yang, L. Xi, W. Zhang, L. Chen, J. Yang, *J. Electron. Mater.* **2009**, *38*, 1397.
[43] D.-K. Ko, Y. Kang, C. B. Murray, *Nano Lett.* **2011**, *11*, 2841.
[44] a) J. Salvador, J. Yang, H. Wang, X. Shi, *J. Appl. Phys.* **2010**, *107*, 043705; b) S. Ballikaya, N. Uzar, S. Yildirim, J. R. Salvador, C. Uher, *J. Solid State Chem.* **2012**, *193*, 31; c) B. Chen, J.-H. Xu, C. Uher, D. T. Morelli, G. P. Meisner, J.-P. Fleurial, T. Caillat, A. Borshchevsky, *Phys. Rev. B* **1997**, *55*, 1476.
[45] J. Yang, M. Endres, G. Meisner, *Phys. Rev. B* **2002**, *66*, 014436.
[46] a) H. Ehrenreich, *J. Phys. Chem. Solids* **1957**, *2*, 131; b) Y. Kajikawa, *J. Appl. Phys.* **2014**, *115*, 203716.
[47] S. Wang, J. Yang, T. Toll, J. Yang, W. Zhang, X. Tang, *Sci. Rep.* **2015**, *5*, 10136.
[48] D. T. Morelli, G. P. Meisner, B. Chen, S. Hu, C. Uher, *Phys. Rev. B* **1997**, *56*, 7376.
[49] X. Zhao, X. Shi, L. Chen, W. Zhang, S. Bai, Y. Pei, X. Li, T. Goto, *Appl. Phys. Lett.* **2006**, *89*, 092121.
[50] Y. Qiu, L. Xi, X. Shi, P. Qiu, W. Zhang, L. Chen, J. R. Salvador, J. Y. Cho, J. Yang, Y. C. Chien, *Adv. Funct. Mater.* **2013**, *23*, 3194.
[51] X. Shi, S. Bai, L. Xi, J. Yang, W. Zhang, L. Chen, J. Yang, *J. Mater. Res.* **2011**, *26*, 1745.
[52] G. Nolas, M. Kaeser, R. Littleton IV, T. Tritt, *Appl. Phys. Lett.* **2000**, *77*, 1855.
[53] D. M. Brown, R. Bray, *Phys. Rev.* **1962**, *127*, 1593.
[54] V. Keppens, D. Mandrus, B. Sales, B. Chakoumakos, P. Dai, R. Coldea, M. Maple, D. Gajewski, E. Freeman, S. Bennington, *Nature* **1998**, *395*, 876.
[55] H. Anno, K. Matsubara, Y. Notohara, T. Sakakibara, H. Tashiro, *J. Appl. Phys.* **1999**, *86*, 3780.
[56] J. Sofo, G. Mahan, *Phys. Rev. B* **1998**, *58*, 15620.
[57] G. Kresse, J. Furthmüller, *Phys. Rev. B* **1996**, *54*, 11169.
[58] J. P. Perdew, K. Burke, M. Ernzerhof, *Phys. Rev. Lett.* **1996**, *77*, 3865.
[59] a) G. Kresse, D. Joubert, *Phys. Rev. B* **1999**, *59*, 1758; b) P. E. Blöchl, *Phys. Rev. B* **1994**, *50*, 17953.